Chalcogenide Letters Vol. 21, No. 1, January 2024, p. 81 - 97

Performance of high sensitive heterojunction CuS/porous silicon photodetector

A. A. Ahmed[a], G. G. Ali[b,*], N. A. Daham[a]
[a]*Department of physics, College of Science, University of Tikrit, Iraq*
[b]*Physics Department, College of Education for Pure Science, University of Mosul, Iraq*

In this work, copper sulfide (CuS) nanostructure was deposited on a porous silicon wafer for the visible light by spray pyrolysis method. Through this, a series of devices were suggested as a part of the deposit concentration of CuS on n-type porous silicon. Simultaneously, the physical features of the attained film were illustrated. FESEM exhibited that the average nanoparticle diameter increased with the concentration of CuS at orientation (100) and was found to be 47.84 nm, 56.36nm and 71.32nm, while the average diameter at (111) orientation was found to be 37.64 nm, 41.46nm, 55.22 nm of 0.1, 0.3 and 0.5M respectively. In addition to the atomic force microscope (AFM) showed the roughness and uniformity of the CuS/PSi fabricated decreased with increasing concentration of CuS, In detail, the attained photo-responsivity and specific detectivity were observed to be 210 mW/A, 340 mW/A and 3×10^{10} Jones, 4.2×10^{10} Jones at orientation (100)using concentration of 0.1M and 0.5M respectively . On the other hand, the photo-responsivity and specific detectivity were observed to be 260 mW/A, 380 mW/A and 1.8 $\times10^{10}$ Jones, 4.5×10^{10} Jones at orientation (111) using concentrations of 0.1M and 0.5M respectively. The presented work shows a substitutional system for an economical and environmentally friendly optoelectronic scheme. The photo-responsive considered to be in a positive linear relationship with the used concentration.

(Received October 31, 2023; Accepted January 11, 2024)

Keywords: CuS, Porous silicon, SEM, XRD, Photodetector

1. Introduction

Copper sulfide CuS exceptional properties make it one of the most essential semiconductor materials. At room temperature, CuS is a p-type semiconducting material with an eV range of 1.5 to 2.7. Copper Sulfide is a direct band gap semiconductor compound that belongs to group II-VI in the periodic table [1,2]. CuS thin films were studied by several technique such as chemical method, sputtering and laser deposed [3,4] . Spray pyrolysis operates by spraying a liquid combination over a substrate that has already been heated, causing a metallic component dissolved in it to break down through pyrolysis [5,6,7]. nanostructured silicon has critically attractive attention due to its unique device structures such as high photoluminescence PL efficiency and large surface area. The visible spectrum generated from porous silicon, regardless of the crystalline Silicon band-gap of 1.12 eV has been attributed to the effects of the quantum size in the nanometer-sized silicon crystallites [8,9,10]. There are various techniques for producing porous silicon such as electrochemical etching, photoelectron chemical etching, chemical etching, and stain etching [11,12]. The combinations of CuS and PSi layer are more crucial because the deposition of high-quality CuS films on a nanostructured silicon surface can provide an excellent identification of lattice constant [13,14]. This work aims to improve the electrical and structural properties of CuS doped on PSi by spray method. The prepared porous silicon samples were then investigated before and after depositing CuS on porous silicon substrates using XRD, AFM & SEM, I-V measurements, and photodetector. The effect of copper sulfide CuS on the porous silicon properties plays an essential part in the emergence of a consistent porosity layer.

* Corresponding author: dr.ghazwan39@uomosul.edu.iq
https://doi.org/10.15251/CL.2024.211.81

2. Experimental method

Photo- electrochemical method was studied to fabricate a porous silicon substrate on n-type silicon with an orientation two parts towards (1 1 1) and (100) and with a resistivity of 1–10 Ω cm. Figure 1(a) shows a setup of the photo electrochemical etching cell. The samples were immersed in Hydrofluoric acid (18% wt) mixed with ethanol (1:1) and tungsten power 100 mw/cm^2 was used. Anodization fixed density is maintained at 15 mA/cm2 and etching times of 5, 10 and 15 min were studied. Additionally, ethanol C2H2OH (99%) is one of the essential wet abilities of the PSi surface. A one-centimeter-diameter rubber O-ring was utilized to enable Teflon cells to come into touch with the silicon layer. The used electricity was consisting of (2) electrodes put under the Si background was the lower electrode and the upper electrode was put on immersed the cell. Following that, CuS films were placed on cleansed glass and substrates made of silicon by the chemical method. An aqueous suspension of extremely pure copper chloride dehydrates (CuCl2·2H2O) and N2S of 0.1, 0.3 and 0.5 M concentration is dispersed first in solution water and then deposited by the solution. Sulphur ions are provided by N2S, and copper ions are provided by CuCl2. The spray flow rate was kept at 30 mL/min whereas the gap between the substrate and the nozzle was altered to 25 cm. The plat temperature is kept at about 250 °C with the help of controlling temperature.

The structural characteristics were performed of the CuS / PSi, X-ray (Bookmark 2) was deployed with a scan speed of 9.9250 [°2Th.]. A Jeol JDS-7381LS scanning electron microscope was utilized. CuS/PSi's current-voltage characteristics were assessed with a halogen lamp and a controlled DC power supply (digital multimeter) under both dark and bright lighting conditions. A monochromator was used to study the photodetector's spectrum responsiveness. The selected ion time was 40 minutes. Next, utilizing a thermal evaporation system (E308W Edwards), aluminum (Al) was deposited on both sides of the CuS/PSi sheet in the form of figure-shaped metal contact electrodes. This was then achieved using a rotary pump and diffusion in a tungsten boat operating at vacuum levels between 10-3 and 10-6 mbar. Figure 1 (b) displays a schematic example of a fabricated device.

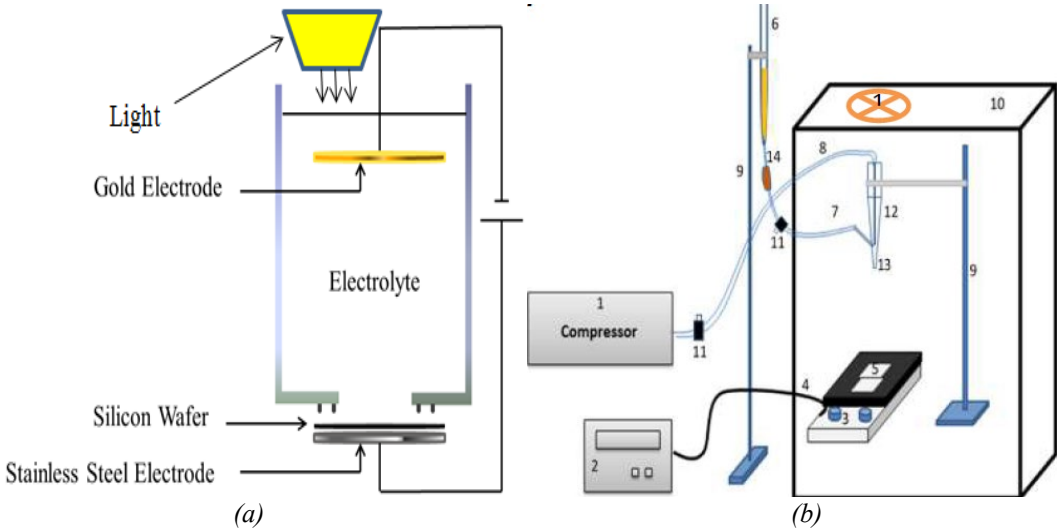

Fig. 1. (a) Set up of Photo electrochemical cell; (b) Set up of spray pyrolysis.

3. Results and discussion

3.1. Structural properties

It was found that Figure 2 (a ,b and c) displays the XRD curves of the deposited CuS nanoparticles on glass wafer for different concentration 0.1 M ,0.3M and 0.5M . All these peaks were obtained corresponding to the hexagonal phase CuS structure of (101), (102) and (103) planes at $2\theta \cong$ 27.58°, 29.17° and 31.73° respectively (JCPDS, No. 00-001-1281) as Table 1. [15]. Figures 3 and 4 (a,b and c) show the XRD pattern of CuS deposed on PSi substrates at orientation (100) and (111)for different concentration 0.1 M ,0.3M and 0.5M at etching time 10 min. Only one highest peak of porous silicon was detected and other small peaks belonged to CuS were noticed, the peaks of PSi (100) and PSi(111) were observed at $2\theta \cong 68.3^{o}$ and 28.3^{o} whereas the CuS noticed at 27.148 ° , 29.2 ° and 31.73 ° corresponded to (101) , (102) and (103) planes respectively.

We can calculate the mean average of crystallite diameter of CuS film by the Scherrer equation as follows [16]:

$$L = \frac{k\lambda}{B\cos\theta} \tag{1}$$

λ is the x-ray wavelength, β is the FWHM and θ is the Bragg angle. It is worth mentioning that the acquired FWHM of CuS and porous silicon increased alongside the CuS concentration increment as Table 2. On the contrary, the crystallite size of CuS decreased at higher concentration value due to interference between CuS and pore layer and cover partially into the pores [17,18].

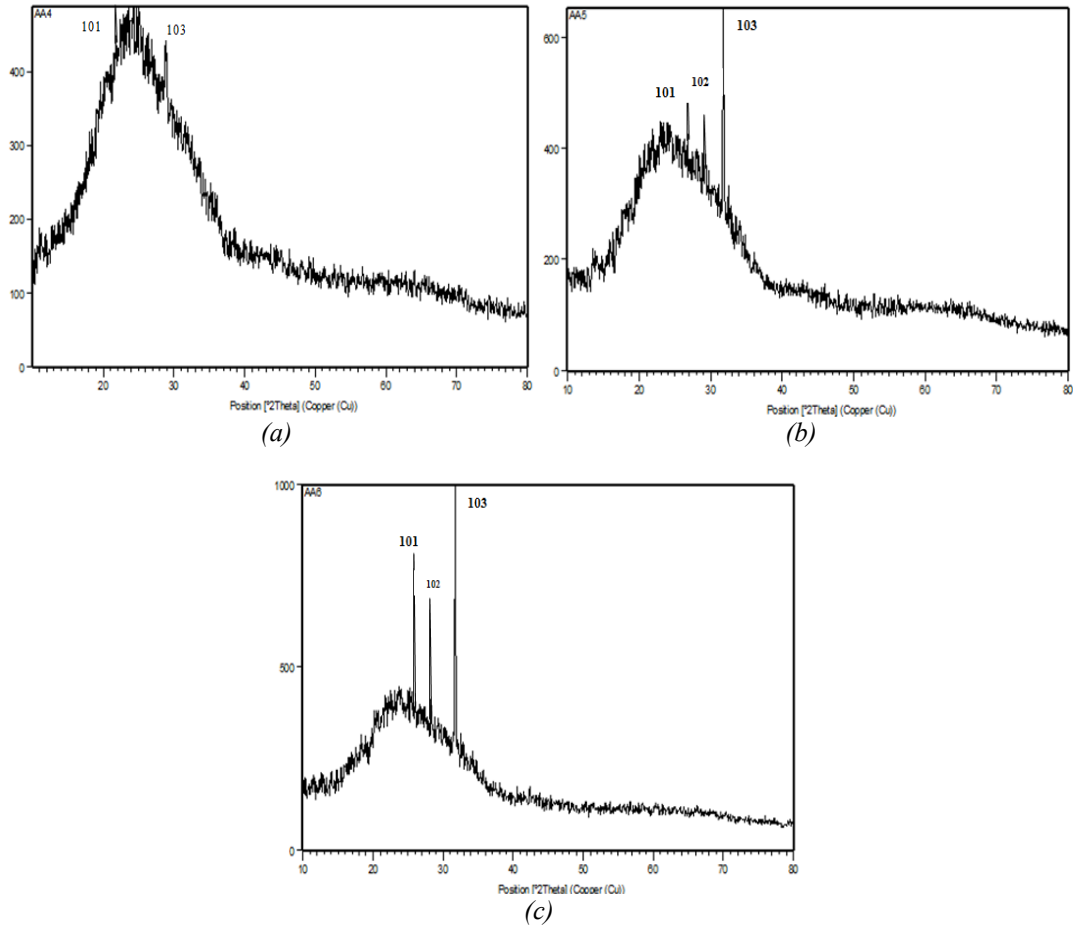

Fig. 2. XRD of CuS thin films deposited on glass wafer at concentrations (a) 0.1M, (b)0.3M and (c)0.5M.

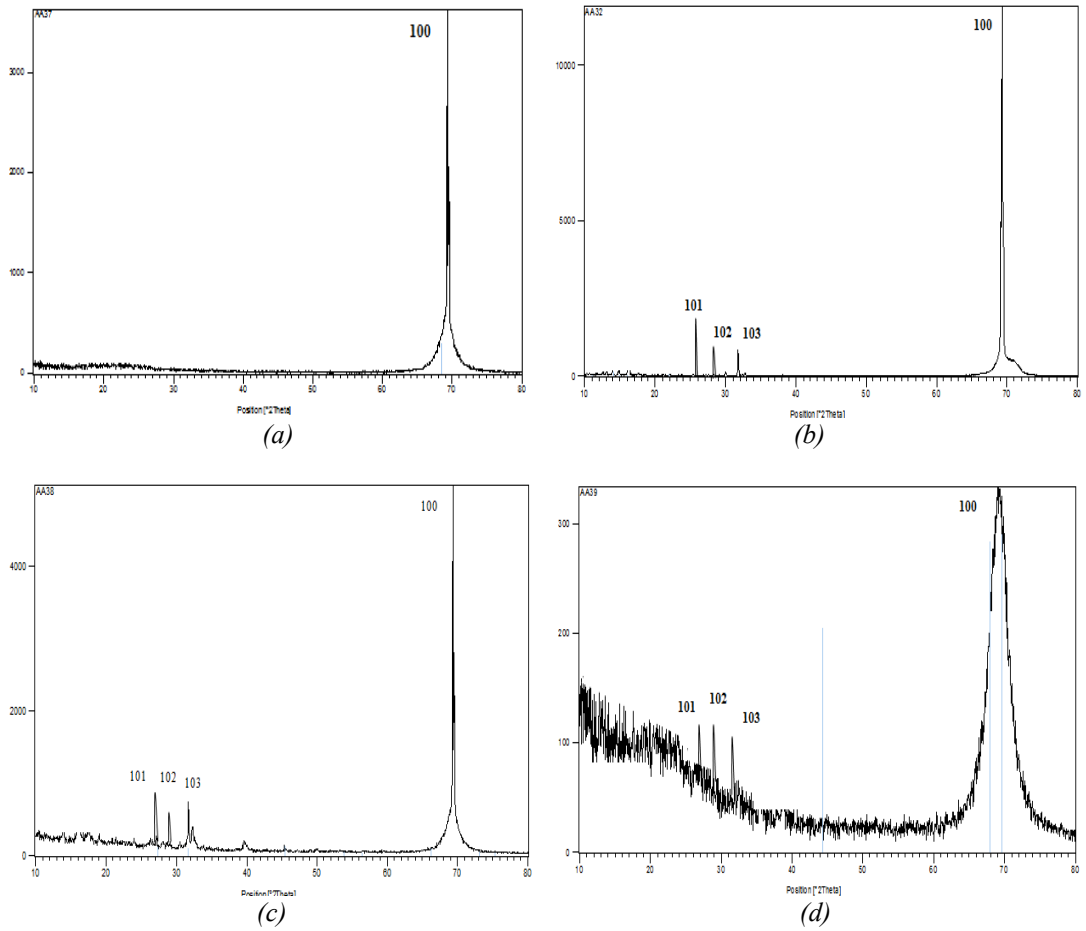

Fig. 3. XRD of CuS thin films deposited on porous silicon wafer (100) at concentrations (a) pure porous silicon, (b) 0.1M, (c)0.3M and (d)0.5M.

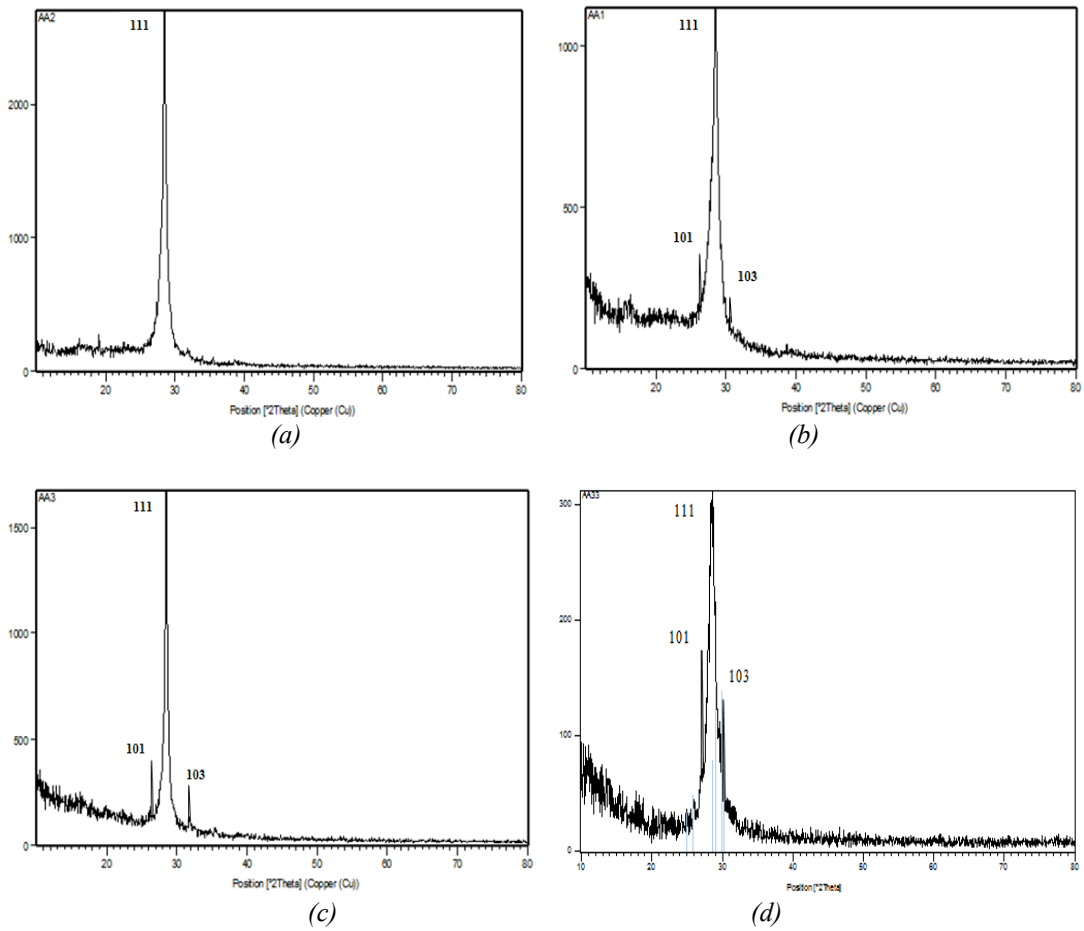

Fig. 4. XRD of CuS thin films deposited on porous silicon wafer (111) at concentrations (a) pure porous silicon , (b) 0.1M,(c)0.3M and (d)0.5M.

Table 1. Crystalline size, FWHM, inter-plane distance (d) of CuS thin films.

Sample	Concentration *(M)*	2θ	*hk l*	*L* (nm)	FWHM (deg)	d (A°)
CuS	0.1	27.58	101	33.52	0.184	2.818
		31.73	103	31.11	0.176	2.763
CuS	0.3	27.58	101	33.23	0.187	2.813
		29.2	102	32.46	0.168	2.842
		31.73	103	30.77	0.179	2.821
CuS	0.5	27.58	101	32.75	0.194	2.863
		29.17	102	31.61	0.184	2.871
		31.73	103	29.62	0.183	2.935

Table 2. Crystalline size, FWHM, inter-plane distance (d) of CuS/PSi hetrostructures.

Sample	Concentration *(M)*	2θ	*hkl*	*L* (nm)	FWHM (deg)	d (A°)
CuS/PSi (100)	0.1	27.6	101	16.45	0.731	1.733
		29.2	102	16.76	0.642	1.711
		31.73	103	17.83	0.623	1.634
		69.3	100	15.43	0.812	1.732
CuS/PSi (100)	0.3	27.6	101	16.11	0.792	1.766
		29.2	102	16.54	0.691	1.789
		31.73	103	17.22	0.722	1.688
		69.3	100	14.76	0.931	1.756
CuS/PSi (100)	0.5	27.6	101	15.87	0.831	1.798
		29.2	102	15.91	0.734	1.82
		31.73	103	16.82	0.782	1.733
		69.3	100	13.68	0.961	1.781
CuS/PSi (111)	0.1	27.6	101	15.44	0.791	1.743
		28.9	111	13.98	0.882	1.788
		31.73	103	14.89	0.782	1.774
CuS/PSi (111)	0.3	27.6	101	15.21	0.831	1.762
		28.9	111	13.15	0.892	1.793
		31.73	103	14.27	0.794	1.781
CuS/PSi (111)	0.5	27.6	101	14.62	0.892	1.772
		28.9	111	12.68	0.942	1.821
		31.73	103	13.61	0.839	1.795

3.2. Surface properties

3.2.1. Atomic force microscope (AFM)

Figure 5 shows the morphology of CuS layers grown at glass substrate was investigated by using Atomic Force Microscopy (AFM) at concentration 0.1 M, 0.3M and 0.5M of 2D& 3D. The irregular distribution of particles is noticed. We observe the non-uniformity in size and shape distribution [19]. Thus, the grains with larger diameters are obtained due to layers aggregation of the grains size [20]. Figure 6 and 7 show CuS deposited on porous silicon at etching time 15 min with 18 %HF and current density 15mA/cm^2 with orientation (100) and (111). The pore diameters increase with increasing of CuS concentration. The roughness decreases with increasing of CuS concentration due to grain sizes cover partially into the pores [21], the roughness and the average diameter of CuS/PSi were noticed in table 3.

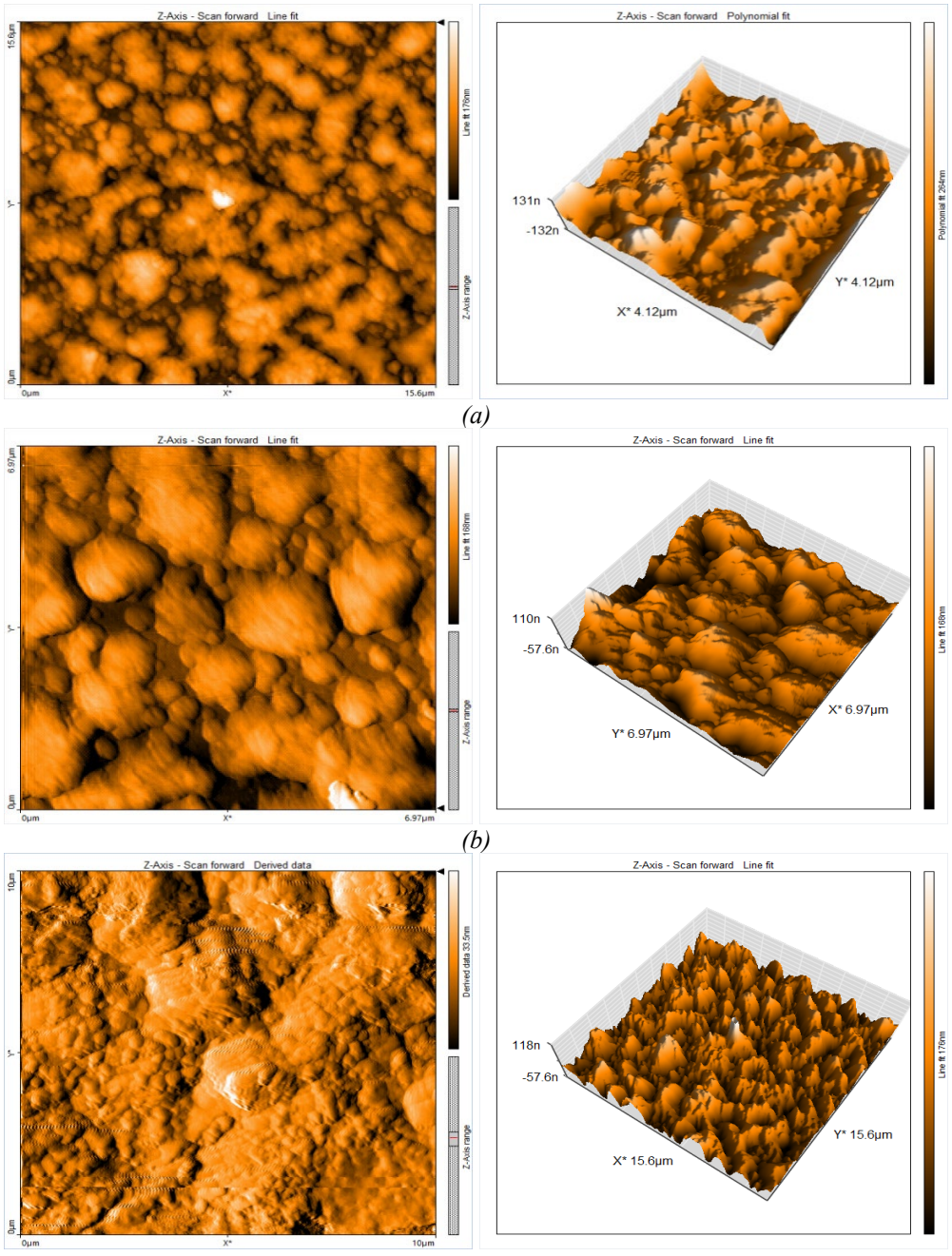

Fig. 5. AFM of CuS thin films deposited on glass wafer at concentrations (a) 0.1M, (b)0.3M and (c)0.5M.

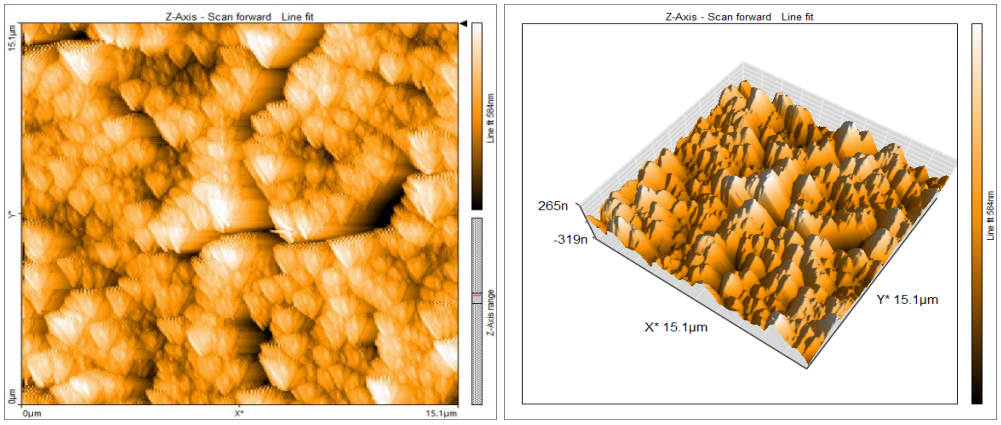

(a)

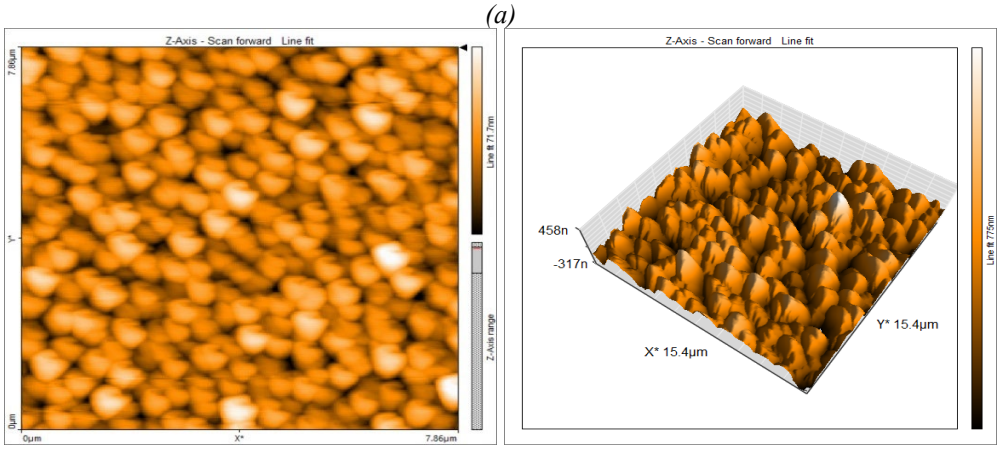

(b)

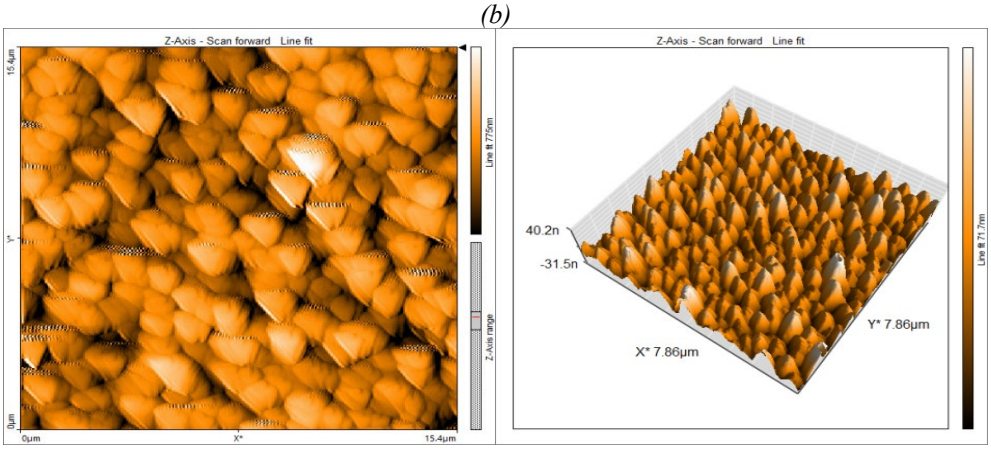

(c)

Fig. 6. AFM of CuS thin films deposited on porous silicon (100) at etching time 15 min. (a) pure porous silicon, (b) 0.1M and (c)0.5M.

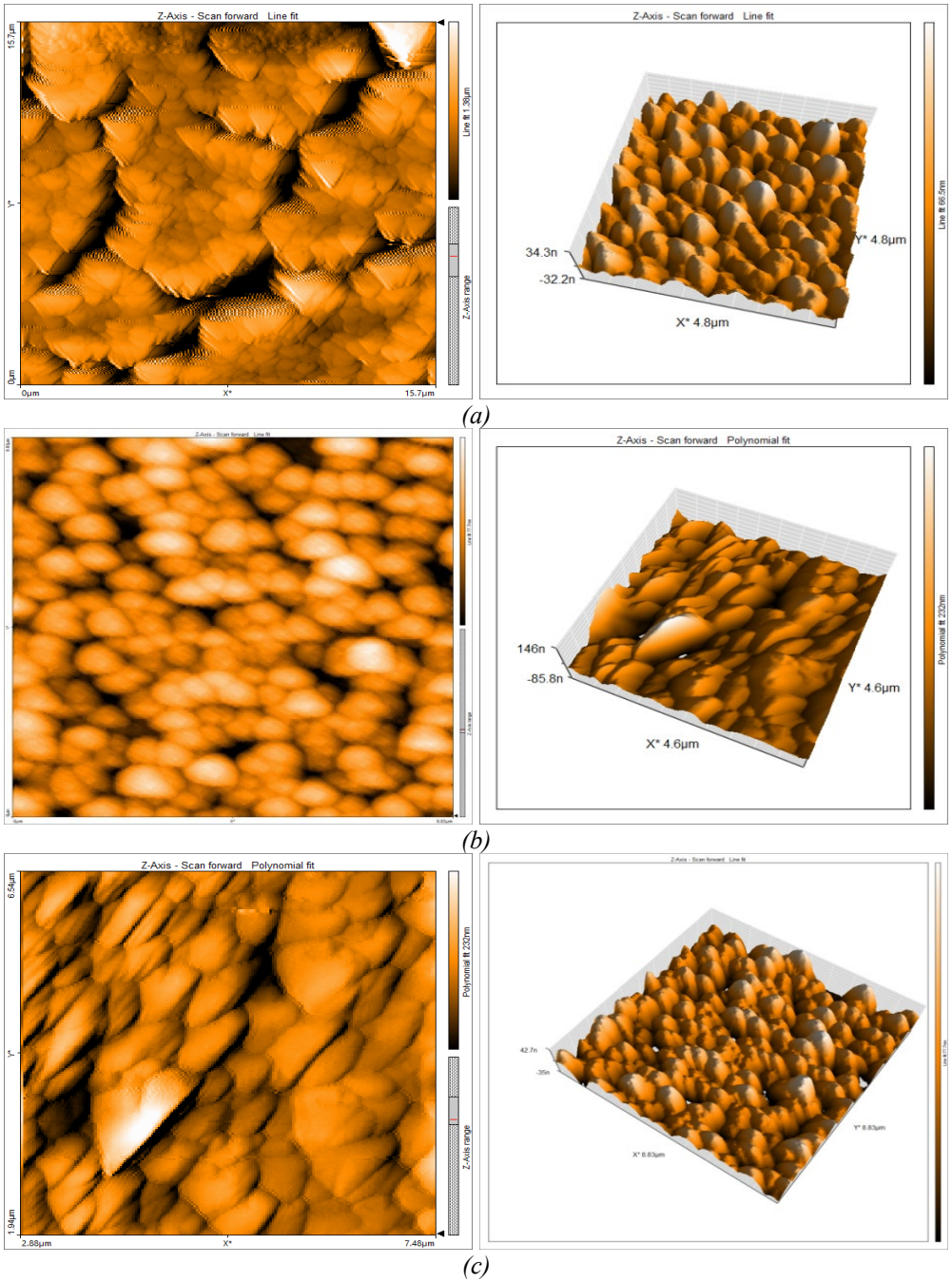

Fig. 6. AFM of CuS thin films deposited on porous silicon (111) at etching time 15 min. (a) pure porous silicon, (b) 0.1M and (c)0.5M.

Table 3. Parameters of Concentration, Roughness Avg., RMS, average diameter of CuS/Psi.

(Concentration g/M)	Orientation	average Roughness (nm)	RMS (nm)	Average Diameter (nm)
0.1	100	2.06	2.23	47.84
0.3		1.89	2.11	56.36
0.5		1.67	1.83	71.32
0.1	111	1.66	1.95	37.64
0.3		1.53	1.88	41.46
0.5		1.34	1.75	55.22

3.2.2. Scanning electron microscope (SEM)

Figure 7 shows CuS deposited on porous silicon with orientation (100) for different concentration 0.1M,0.3M and 0.5M. It should be noted that, as Figure 7a illustrates, an excess of pores at the top surface and the additional chemical dissolution in HF caused a sponge-like structure to form during the anodization process [22]. It can be observed that the pore diameters rise with increasing CuS concentrations such as Figure 7b, c and d. The distribution of PSi's closest neighbor pores can be significantly influenced by its surface shape [23]. The pore distribution follows a regular pattern. CuS is deposited at several concentrations (0.1M, 0.2M, and 0.3M) over porous silicon with orientation (111) as seen in Figure 8(a), (b), (c), and (d). The final PSi structures can be manipulated by the fabrication circumstances. Compared with orientation (100) samples, pores with greater sizes are obtained. Additionally, the pores feature cluster and star-shaped structures rather than spherical ones, which may be the result of the lattice being moved. In the dense displacement zones, gaps and clusters form. Following the initial formation of Si interstitial and vacancies at the surface, a migration of the defects takes place. Consequently, the effect of neutron irradiation may enhance the PSi surface's homogenous porosity distribution [24].

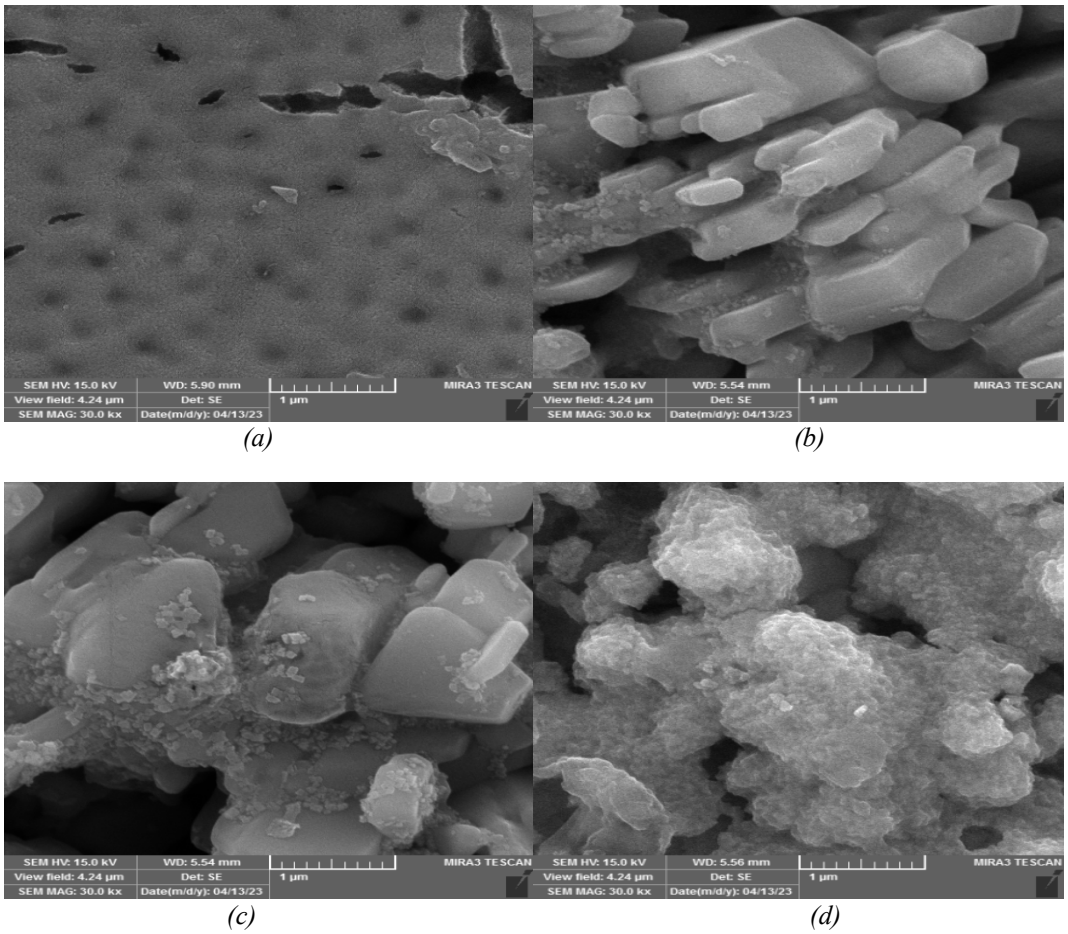

Fig. 7. SEM of CuS thin films deposited on porous silicon (100) at etching time 15 min. (a) pure porous silicon, (b) 0.1M, (c) 0.1M and (d) 0.5M.

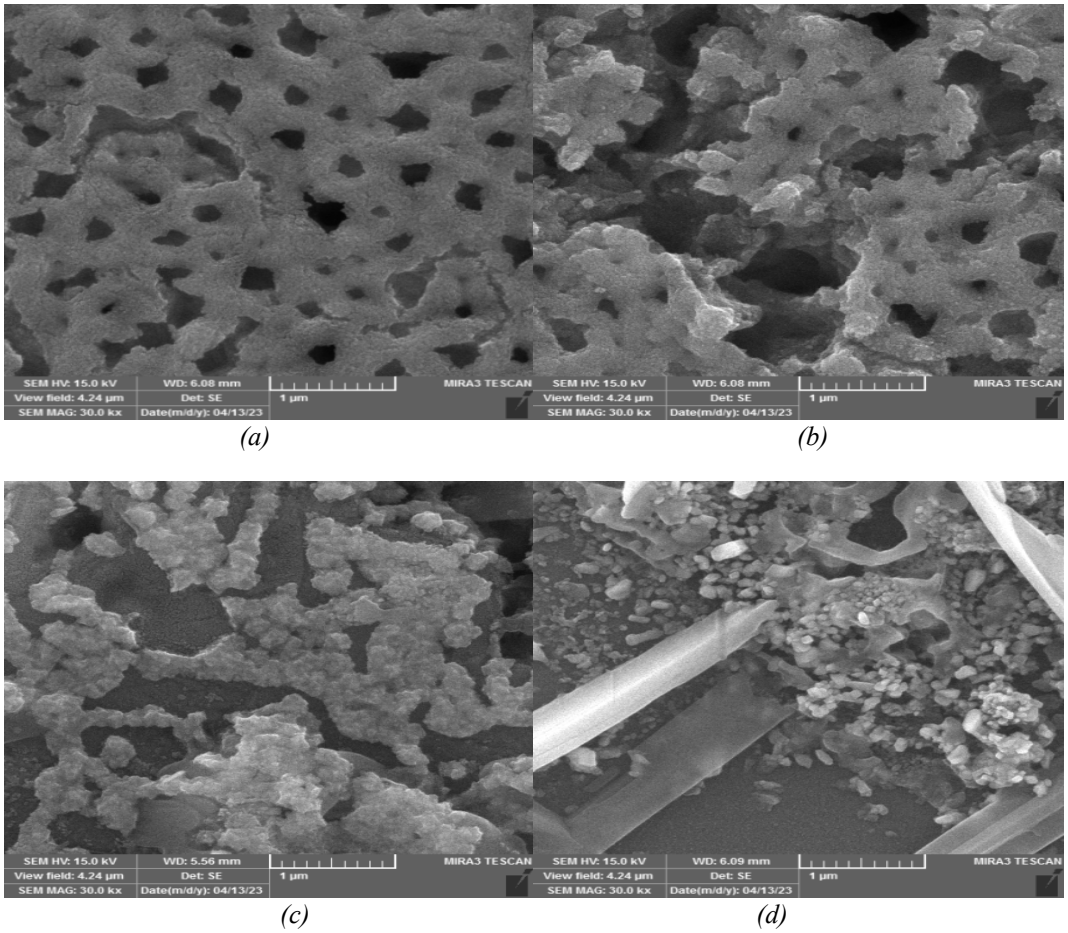

Fig. 8. SEM of CuS thin films deposited on porous silicon (111) at etching time 15 min. (a) pure porous silicon, (b) 0.1M, (c) 0.1M and (d) 0.5M.

3.3. I-V measurements

According to the Hall measurement, the Hall coefficient of CuS was p-type. The I–V values under dark and illumination condition of the fabricated CuS/porous silicon photodetector at various concentrations (0.1, 0.3, and 0.5 M) for both orientations (111) and (100) are shown in Figures 9 and 10. The acquired I-V curves indicate the presence of the heterojunction of CuS/ porous silicon and have rectification behavior. Afterwards, a rise in carrier production and absorbed photons caused an increase in current at a higher bias voltage [25]. Increased reverse bias voltage also produced high current values, which may have been caused by an increase in the depletion layer width. This increased internal electric field, in turn, increased the likelihood of electron-hole separation. It is also important to note that, as Table 4 illustrates, a rise in CuS content was linked to an increase in dark and photocurrent [26,27].

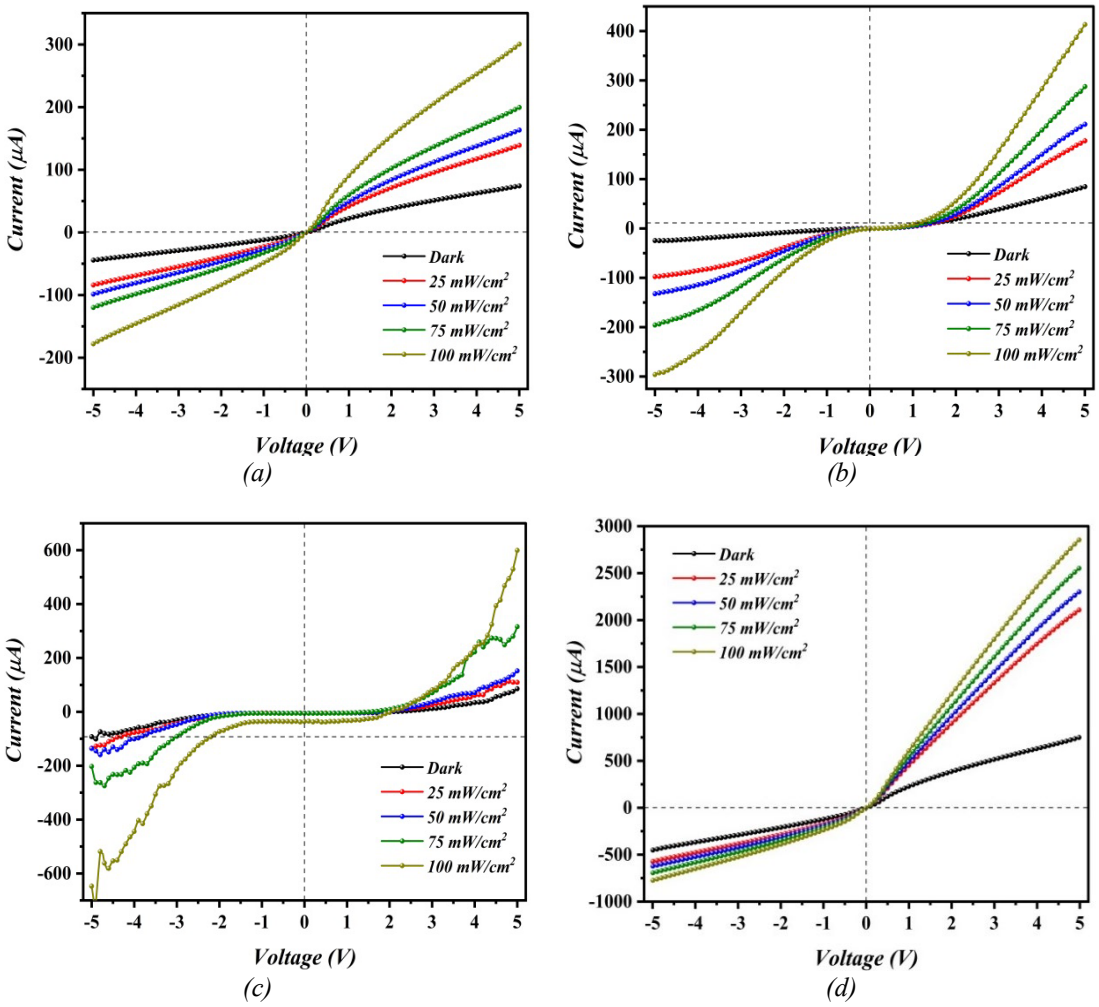

Fig. 9. I-V measurements of CuS thin films deposited on porous silicon (111) at etching time 5 min. (a) pure porous silicon, (b) 0.1M, (c) 0.1M and (d) 0.5M.

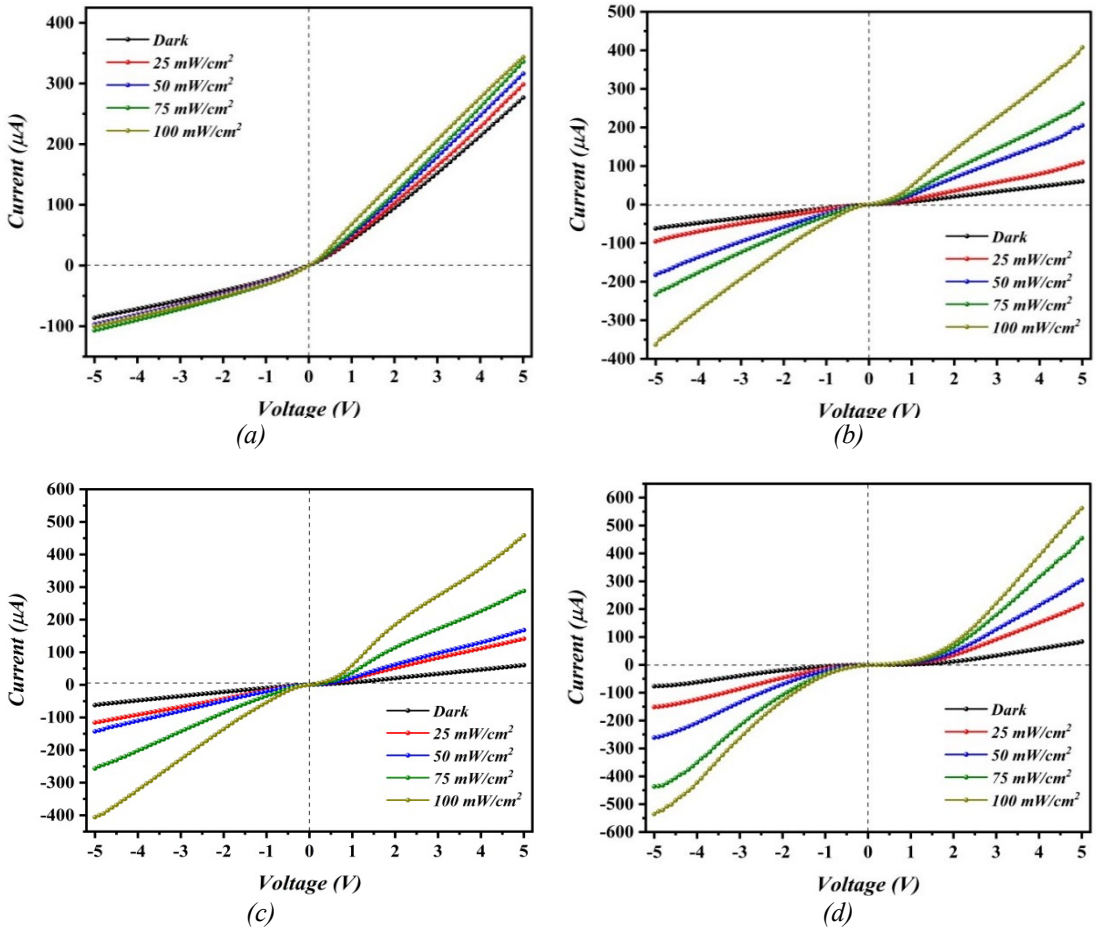

Fig. 10. I-V measurements of CuS thin films deposited on porous silicon (100) at etching time 5 min. (a) pure porous silicon, (b) 0.1M, (c) 0.1M and (d) 0.5M.

Table 4. Value of ideality factor, barrier height of PSi with different concentration at etching time 5min.

PSi with orientation (100)				PSi with orientation (111)			
Concentration (M)	J_s (μA)	n	Φ (eV)	Concentration (M)	J_s (μA)	n	Φ (eV)
0.1	1221	1.57	0.55	0.1	1947	1.77	0.41
0.3	605	1.89	0.59	0.3	810	2.2	0.49
0.5	95	2.14	0.72	0.5	241	2.54	0.56

Figure 11 (a and b) illustrated scale of the dark current as a function of concentration at 4.5 bias voltage with orientation (100) and (111). The measured linear rise in output dark current with increasing CuS concentration from this an increase in photo-excited electrons at higher power could be the explanation for singularity, leading to an increase in the number of electrons in the CB of the deposited film [28].

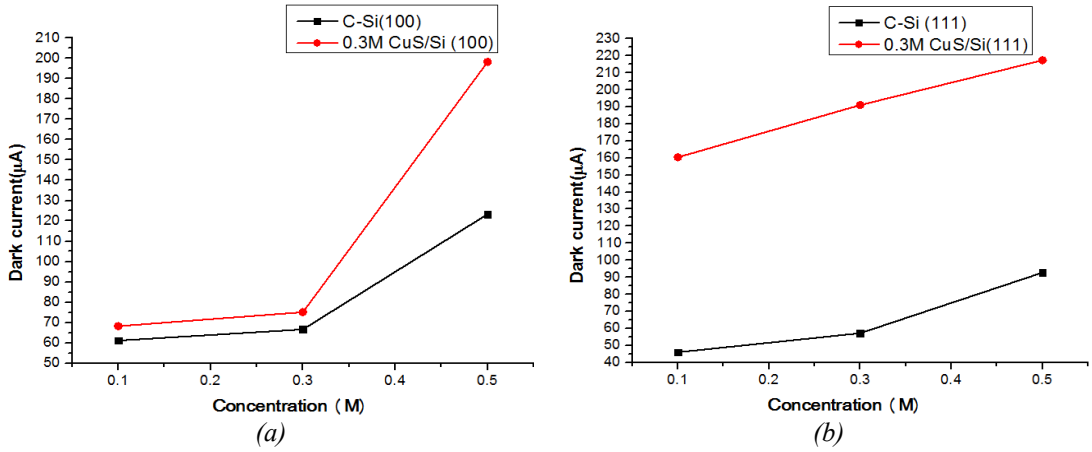

Fig. 11. Dark current as a function of concentration at orientation (a) (100) and (b) (111).

3.4. Photodetector

The photo-responsivity (R) is known as the ratio of output photocurrent to the applied illumination power.

$$\boldsymbol{R = \frac{I_{ph}}{P \times A}} \tag{2}$$

Identical patterns of behavior were noted in the specific detectivity profile (D∗):

$$\boldsymbol{D^* = \frac{R(\lambda)}{\sqrt{2qJ_{dark}}}} \tag{3}$$

where $\boldsymbol{J_{dark}}$ is the dark current density and q is the electron charge [29,30]. Figures 12 and 13 (a and b) show the responsivity (R) and detectivity profile ($D*$) *as* a function of the wavelength of CuS/PSi for different orientation (111) and (100). There are three peaks , first peak at high response in the ultraviolet region for both R and $D*$ were observed particularly at 500−600 nm , this is due to junctions: CuS/PSi and PSi/CSi, second region at low response at 700-800 nm , However, the third region, 800-900 nm, showed a considerable rise in the previously indicated values. notably, the obtained values of R and D∗ showed a rising trend in response to high CuS concentration during the deposition process, which raises the quantity of photons in the depletion zone. High values of R and DTM were obtained when the concentration of CuS was raised from 0.1M to 0.5M. This might be attributed to the improved crystal quality of the deposited CuS layer at high concentration [31]. Figure 14 (a and b) illustrates the CuS/PSi photodetector's quantum efficiency as a value of wavelength. The high value of quantum efficiency of CuS/PSi at orientation (111) and (100) were found to be 78% and 69 % at wavelength 580 nm with bias voltage of 4.5 V and at the near infrared range, it drops to 25% and 30%, respectively. The cause of this can be capture centers existing at interface PSi/CSi. The value efficiency of CuS/PSi photodetector of (111) samples are higher than (100) which are belonged to reconfiguration of structure [32,33,34].

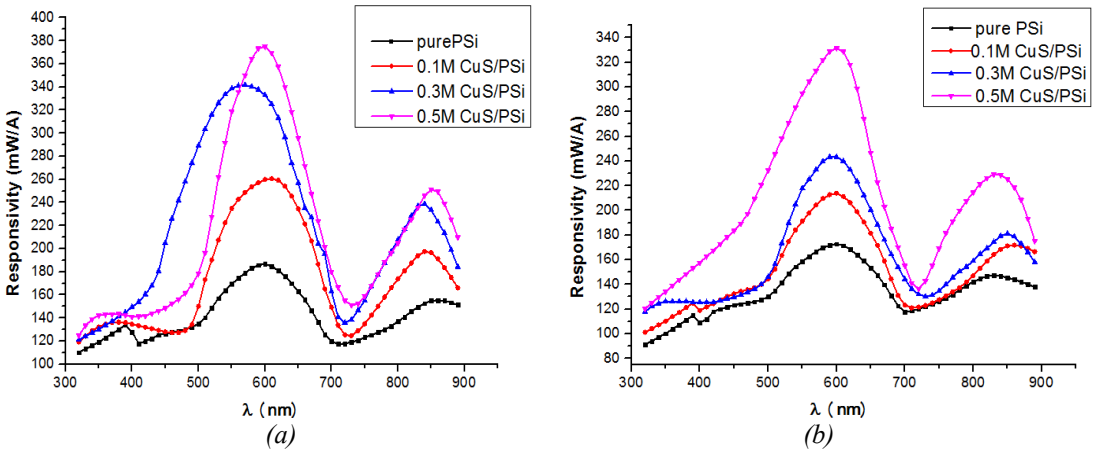

Fig. 12. Photo-responsivity of CuS/PSi heterojunction of (111) and (100) at etching time 5 min. (a) pure porous silicon, (b) 0.1M, (c) 0.1M and (d) 0.5M.

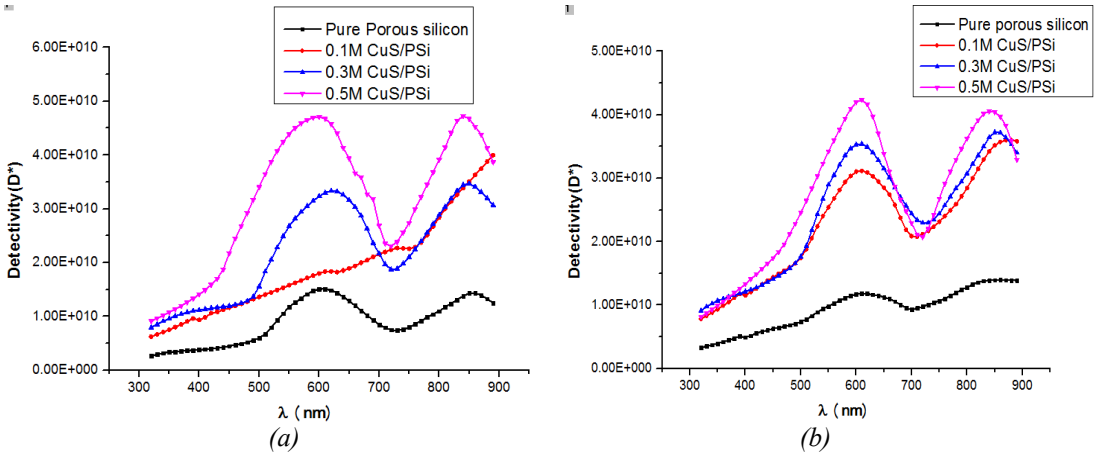

Fig. 13. Detectivity of CuS/PSi heterojunction at etching time 5 min, (a) orientation (111) and (b) orientation (100).

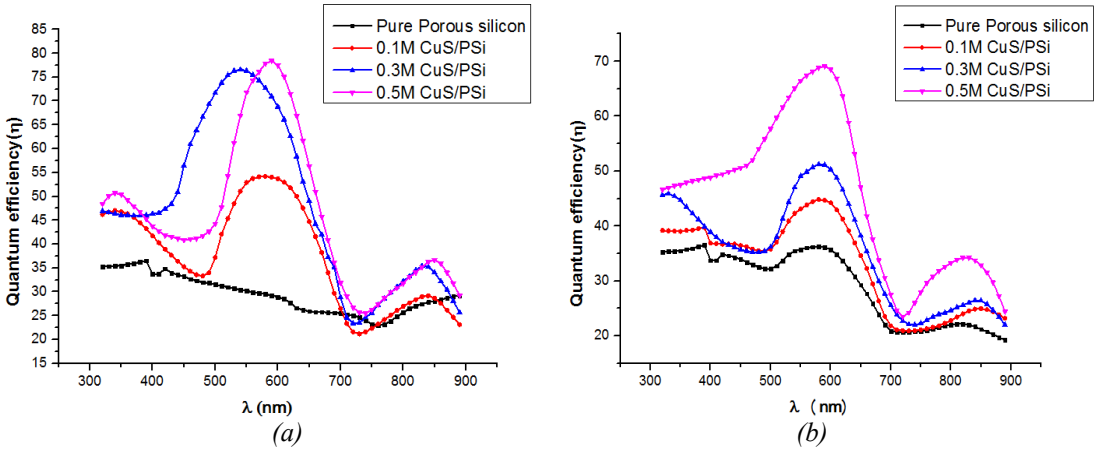

Fig. 14. Quantum efficiency of CuS/PSi heterojunction at etching time 5 min, (a) orientation (111) and (b) orientation (100).

4. Conclusion

Copper sulfide nanostructure deposited on porous silicon photodetector was successfully fabricated by spray pyrolysis technique, with respect to the utilized concentration of CuS. XRD patterns exhibit hexagonal phase CuS structure. The surface analysis revealed the existence of spherical morphology and the roughness of the CuS/PSi decreased with increasing concentration of CuS . Furthermore, photodetector behavior showed that D* at pure porous silicon and 0.5 M with (100) and (111) were found to be 0.8×10^{10} Jones, 1×10^{10} , 4.2×10^{10} Jones and 4.5×10^{10} Jones respectively. Besides, the quantum efficiency of CuS/PSi photodetector of (111) samples are higher than (100) which are belonged to reconfiguration of structure. Watchful modification of the experimental circumstances can help create an ideal porous silicon structure.

References

[1] S. Yadav, P. K. Bajpai, Soft Nanosc, Letters, 8(2), 9-19. (2018); https://doi.org/10.4236/snl.2018.82002

[2] S. T. Kassim, H. A. Hadi, R. A. Ismail, Optik, 221(2), 165339 (2020); https://doi.org/10.1016/j.ijleo.2020.165339

[3] S. Gunasekaran, D. Thangaraju, R. Marnadu, J. Chandrasekaran, M. Shkir, A. Durairajan, M. Elango, Sensors and Actuators A: Physical, 317(4), (2021); https://doi.org/10.1016/j.sna.2020.112373

[4] J. Zhang, H. Shen, Y. Xu, B. Xu, Y. Feng, J. Ge, Y. Li, Surfa. and Interfaces 26(1), (2021); https://doi.org/10.1016/j.surfin.2021.101430

[5] R. A. Rasool, Ghazwan G. Ali, N. A. Hussein Digest Journal of Nanomaterials and Biostructures, 14(3), pp. 743 - 750,(2019).

[6] Y. Xu, H. Shen, J. Zhang, Q. Zhao, Z. Wang, B. Xu, W. Zhang, J. of Alloys and Compounds, 884(12), (2021); https://doi.org/10.1016/j.jallcom.2021.161121

[7] A. K. Katiyar, A. K. Sinha, S. Manna, R. Aluguri, S. K. Ray, Phys. Chemistry Physics, 15(48), 20887-20893, (2013); https://doi.org/10.1039/c3cp53603c

[8] Rehab Joko Hussin, Ivan B. Karomi, Results in Optics, 12 (2023) 100452. https://doi.org/10.1016/j.rio.2023.100452

[9] Al-Ghamdi, M.S., Bahnam, R.Z., Karomi, I.B., Heliyon , 8 (9) (2022) e10587. https://doi.org/10.1016/j.heliyon.2022.e10587

[10] Abdulkahliq A. Sulaiman, Ghazwan Gh. Ali, Ahmed Izzalddin Thanon, Journal of Nanostructure, 12(1), p 1-11 (2022).

[11] Sheng .Y. Wang, Wei. W., Zu. H. Lu, Elsevier, B103, p.p.184-188 (2003).

[12] G. G. Ali, M. A. Ahmed, A. A. Sulaiman, Structural properties of AuNPs/PSi nanostructure, Digest Journal of Nanomaterials and Biostructures 17(2), p. 473 - 480 (2022); https://doi.org/10.15251/DJNB.2022.172.473

[13] A. H. Mustafa, Sci. in Applied physics ,University of Technology, (2006).

[14] L. Isac, I .Popovici, A. Enesca, A. Duta, Elsevier 3(2), 71-78 (2010); https://doi.org/10.1016/j.egypro.2010.07.013

[15] T. A. Aswad, T. A. Abbas, G. G. Ali, Digest Journal of Nanomaterials and Biostructures 16(3), p. 831 - 838(2021); https://doi.org/10.15251/DJNB.2021.163.831

[16] P. V. Nho, P. H. Ngan, Hanoi University of Science 9 (10), p.397- 402 (2012) .

[17] A. Mehdi, H. Eshghi, M. B. Mohagheghi, Elsevier 258(2), pp. 5733-5738 (2012); https://doi.org/10.1016/j.apsusc.2012.02.079

[18] D. Shin, S. Lee, D. R Kim, J. H. Park, Y. Kim, W. J. Choi, Energies 13(3), 688 (2020); https://doi.org/10.3390/en13030688

[19] N. P. Huse, A. S. Dive, K. P. Gattu, R. Sharma, Materials Sci. in Semiconductor Proc. 67(2), 62-68 (2017); https://doi.org/10.1016/j.mssp.2017.05.010

[20] Y. E. Firat, H. Yildirim, K. Erturk, A. H. Peksoz, Applied physics 3(1), 2017; https://doi.org/10.1155/2017/2625132

[21] J .Santamaria, E. Iobrra, Vacuum 37 (516), p.p.437-439 (1987); https://doi.org/10.1016/0042-207X(87)90329-0

[22] S. B. Gadgil, R. Thangaray, J. Phys. D Appl. Phys. 20(2), p.p.112 -115 (1987); https://doi.org/10.1088/0022-3727/20/1/017

[23] C. Nascu, I. Pop, V. Ionescu, E. Indrea, I. Bratu, Elsevier 32(3), pp.73-77 (1997); https://doi.org/10.1016/S0167-577X(97)00015-3

[24] I. Wuled, Y. Chan Kang, T. Komiya, K. O. Kuyama, N. Tphge, Research Gate, part 2, 3(37), p.p.288- 290 (1998).

[25] Ç. Taşdemirci, Optical and Quantum Electronics 51(7), pp. 245-255 (2019); https://doi.org/10.1007/s11082-019-1963-0

[26] F. A. Sabah, N. M. Ahmed, Z. Hassan, M. A. Almessiere, Materials Science in Semiconductor Processing, 63(2), 269-278 (2017); https://doi.org/10.1016/j.mssp.2017.02.032

[27] H. S. Rangel, A. Castillo, J. Hernández, J. Paz, H. Montes, P. García, C. R. González, (2015).Chalcogenide Letters, 12(6), 381-387

[28] A. K. Sahoo, P. Mohanta, A. S. Bhattacharyya, Materials Science and Engineering 73(1), p. 012123, IOP conference 3(2015); https://doi.org/10.1088/1757-899X/73/1/012123

[29] M. A., Sangamesha, K. Pushpalatha, G. L. Shekar, S. Shamsundar, International Scholarly (2013); https://doi.org/10.1155/2013/829430Research Notices 3(2)

[30] D. Shin, S.Lee, D. R Kim, J. H. Park, Y. Kim, W. J. Choi, D. Hwang, Energies, 13(3), 688-700 (2020); https://doi.org/10.3390/en13030688

[31] O.Erken, M. Gunes, F. Kirmizigul, C. Gumus, Optik 168(4), 884-891 (2018); https://doi.org/10.1016/j.ijleo.2018.05.031

[32] S. Cruz, J., Mayén, S. A. Paraguay, F. Zelaya, O. Castanedo, T. Delgado, International Journal of Photoenergy 4(1) (2013); https://doi.org/10.1155/2013/178017

[33] R. Zeinodin, J. Sheini, M. Cheraghizade, Materials Science in Semiconductor Processing 123(2), 105501 (2021); https://doi.org/10.1016/j.mssp.2020.105501

[34] Yasir Y. K., Ghazwan Gh. A., Marwan H.Y. Iraqi J. of Sci., 62(1), 130-137 (2021); https://doi.org/10.24996/ijs.2021.62.1.12